COMBINATION OF TLS AND SLAM LIDAR FOR LEVEE MONITORING

Dimitrios Bolkas[1*], Matthew O'Banion[2], Christopher J. Belleman[3]

[1]Department of Surveying Engineering, Pennsylvania State University, Wilkes-Barre Campus, Dallas, PA – dxb80@psu.edu
[2]Department of Geography & Environmental Engineering, United States Military Academy at West Point, West Point, NY – matthew.obanion@westpoint.edu
[3]Luzerne County Flood Protection Authority, Kingston, PA, – cbelleman@lcfpa.org

Commission III, WG III/7

KEY WORDS: terrestrial laser scanning, SLAM LiDAR, point clouds, drift correction, levees, monitoring.

ABSTRACT:

Monitoring of engineering structures is important for ensuring safety of operation. Traditional surveying methods have proven to be reliable; however, the advent of new point cloud technologies such as terrestrial laser scanning (TLS) and small unmanned aerial systems (sUAS) have provided an unprecedented wealth of data. Furthermore, simultaneous localization and mapping (SLAM) is now able to facilitate the collection of registered point clouds on the fly. SLAM is most successful when applied to indoor environments where the algorithm can identify primitives (points, planes, lines) for registration, but it can be problematic in outdoor settings where there is absence of constructed features. This work includes the collection of SLAM-based LiDAR data along a levee for the purpose of inspection and monitoring. Due to the outdoor setting and absence of man-made features, the resulting point cloud was considerably distorted due to erroneous drift in sensor orientation. A correction algorithm is proposed that relies on reference TLS point cloud data to remove drift distortions identified in the SLAM LiDAR. Results indicate an alignment between the corrected SLAM LiDAR and TLS data of around ±10cm, which is sufficient for general inspection and multi-epoch monitoring of levees. The algorithm is based on common points identified in the TLS and SLAM data and necessitates that the SLAM LiDAR is collected in individual, one-way lines to allow correction of distortions as a function of distance from the starting point. This approach increases the efficiency of LiDAR-based levee monitoring by reducing the time required to survey the levees.

1. INTRODUCTION

Monitoring of engineering structures (e.g., dams, levees, and bridges) is an important surveying task for ensuring safety of operation and integrity of structures. Monitoring of structures and deformation estimation has significantly been enhanced in the past decade thanks to the development of point cloud technologies such as terrestrial laser scanning (TLS) and small unmanned aerial systems (sUASs) (e.g., Bakula et al., 2016; Bakula et al., 2020; Akiyama et al., 2021). With respect to levee monitoring, these technologies provide faster data acquisition and dense point cloud datasets that can support high resolution quantitative analyses. In recent years, simultaneous localization and mapping (SLAM) light detection and ranging (LiDAR) has experienced rapid advancement and application in surveying for the kinematic acquisition of dense point clouds. Currently, SLAM LiDAR works best in indoor environments thanks to the existence of geometries that can be modelled mathematically (e.g., walls can be represented by planes, and the intersection of two walls as lines) and distinct features (such as corners and other well-defined points or features). In such indoor environments, SLAM algorithms keep track of the geometry and deliver point clouds with cm-level accuracy (Leica Geosystems 2021; Zou et al., 2021). Use of SLAM in outdoor environments can become challenging in the absence of well-defined geometries and correspondences, which can lead to decreased accuracy and in some cases, failure of the SLAM algorithm (Lenac et al., 2017). In the case of decreased SLAM performance, the resulting point cloud may present large mismatches due to drifts of the inertial measurement unit (IMU). For instance, Akiyama et al. (2021) used SLAM LiDAR for monitoring an 800 m levee section and the achieved accuracy was around 0.3 m to 0.5 m due to accumulated errors.

The efficient data collection (simply walking with the sensor) provided by SLAM LiDAR makes this technology attractive for inspection and monitoring of levees. Conversely, TLS would require numerous, time-consuming setups, especially for LiDAR points to achieve higher vegetation penetration and reach the ground (e.g., Bolkas et al., 2021). While sUAS surveys offer an efficient solution for capturing levee geometry, inefficiencies are often introduced through the flight approval process and the nature of surveying long linear alignments. In the case of a levee alignment, numerous flights from various take-off locations would likely be required in order to maintain visual line of sight of the aircraft at all times. Additionally, the inherent hazards of sUAS operation must be considered in situations where non-participating personnel and/or personal property may be present. For this reason, this paper explores the combination of TLS and SLAM LiDAR for the inspection and monitoring of levees. As discussed later in this paper, the TLS dataset is used as a reference for registration and correction of the SLAM LiDAR point clouds. Future data acquisitions will be based only on the SLAM LiDAR data, using the reference TLS for registration and correction of

* Corresponding author

the SLAM data, reducing the time spent in the field and increasing monitoring efficiency. Since the TLS and SLAM LiDAR data were collected at different times, they are also compared to quantify any geometric changes over time. An algorithm was developed for the co-registration of the SLAM and TLS LiDAR point clouds followed by removal of geometric distortion identified in the SLAM LiDAR data. The following sections provide information about the study area, the acquisition of the TLS and SLAM LiDAR datasets, and the geometric distortions identified in the SLAM LiDAR data. Next, we present the algorithm developed for the co-registration and distortion removal of the SLAM LiDAR, results of the TLS and SLAM point cloud comparison, and the conclusions of this work.

2. STUDY AREA AND DATASETS

2.1 The Kingston Levee System

The Luzerne County Flood Protection Authority is tasked with the operation and maintenance of the 26-km long Wyoming Valley Flood Risk Management Project, along the Susquehanna River near Wilkes-Barre, Pennsylvania. A component of this flood protection system is the Kingston to Edwardsville levee reach which is located along the east bank of the river. The study area is located near the upstream portion of this levee reach, and the segment in question has a length of about 750 m, width that ranges from 40 m to 50 m, and a height of about 8 m.

2.2 Control Network

A network of twenty (20) control points was established to facilitate TLS and future sUAS surveys (Figure 1). Two of the twenty control points are located at a distance of 200 m from the study area to provide external control for the multi-epoch datasets. The control points were surveyed using rapid static Global Navigation Satellite System (GNSS) observations. Standard deviations of the post network adjustment were at the 2-3 mm level, for both horizontal and vertical coordinates. Considering a miscentering at the level of few-mm, then the accuracy of the control points is expected to be at the 1 cm level.

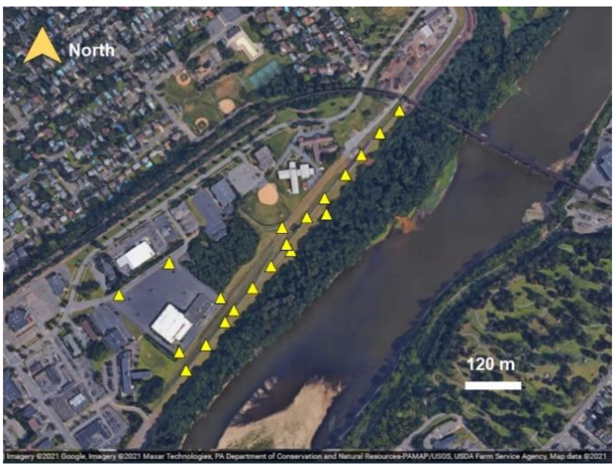

Figure 1. Study site and control network in Kingston, Pennsylvania. Triangles depict the approximate location of control points.

2.3 TLS Datasets

The TLS dataset was acquired using a Leica Scan Station P50. The San Station P50 is a panoramic scanner that offers fast scan rates of up to one million points per second (Leica Geosystems 2021b). Scanner range accuracy is 1.2 mm + 10 ppm, and scanner angular accuracy is 8″ horizontal and 8″ vertical. The scanner has a dual axis compensator with an accuracy of 1.5″.

TLS registration was achieved through resection at a minimum of three control points for redundancy. Standard deviations of the resection solutions did not exceed the 1 cm level, with an average of ± 4 mm. This indicates that positioning accuracy of the point cloud is at the 1 cm level, and most error in the point cloud will originate by data gaps due to line-of-sight obstructions and laser penetration of vegetation, which can deteriorate accuracy (e.g., Bolkas et al., 2021).

The scanner resolution was set to 1 cm at 20 m, and a total of 26 scans were collected, with an average ground point spacing of 3 cm. However, due to line-of-sight obstructions, some data gaps exist at the top of the levees, which are up to around 0.5 m in largest dimension. Only a few scans were collected on the top of the levees, as most of the focus was placed on identifying changes at the foot of the levees.

2.4 SLAM LiDAR Datasets

In addition to the TLS scans, SLAM LiDAR was collected using a Leica BLK2GO system. The Leica BLK2GO uses a combination of LiDAR, visual SLAM, and an inertial measurement unit (IMU) to facilitate kinematic LiDAR collection. The BLK2GO uses both visual- and LiDAR-based SLAM to track the scanner's movement in space. The visual SLAM capability relies on the three integrated panoramic cameras to track the scanner's movement in space and the IMU is used to calculate the change in position and orientation throughout the survey (Leica Geosystems 2021a).

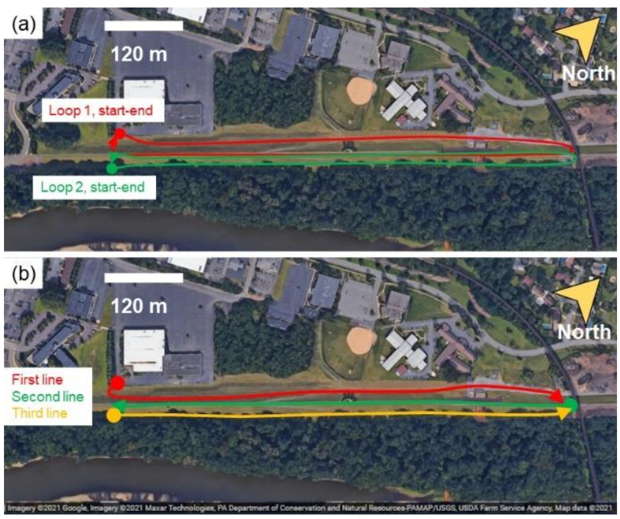

Figure 2. SLAM data collection (a) using a closed loop acquisition scheme (ending survey at the starting point) (b) using multiple linear surveys without loop closure.

The BLK2GO scanner has an indoor accuracy of 1 cm; however, outdoor accuracy can vary greatly due to the lack of easily identifiable features, presence of vegetation, and variable lighting conditions. In addition, for SLAM kinematic LiDAR systems, the pace of forward movement can affect accuracy. It is important to maintain a relatively slow and consistent pace to allow the algorithm to correctly identify correspondences in the surrounding environment. The manufacturer also recommends that a survey closes the loop by returning to the beginning point. Closing the loop allows for the SLAM algorithm to estimate a misclosure and correct for IMU drifts (Leica Geosystems, 2020). These requirements may be easy to satisfy in indoor environments; however, it becomes more challenging and, in some cases, impractical in outdoor environments. In this study, the levees span for hundreds of meters having a predominantly linear shape. Furthermore, for this study closing the loop did not perform better than individual survey lines. Two SLAM scans forming loops were collected (Figure 2a). Because of the requirement to walk slow, it took about 20 minutes to walk each loop. Three linear SLAM scans were also collected, one on the protected side, one on the top of the levee, and one on the river side (Figure 2b).

3. DISTORTION IN SLAM LIDAR

SLAM relies on the identification of similarities and common geometries or features in real time to register the LiDAR points as the user walks / scans. If the process of identifying such similarities and correspondences deteriorates with time / distance, so will the registration accuracy of the point cloud. The magnitude of registration inaccuracies (inaccuracies in orientations and translations) will depend on distance or time.

Most levee alignments are laid out in a linear fashion following the boundaries of a river. Such outdoor environments often have few or no distinct features (e.g., buildings, bridges, walls) and they are mostly characterized by low vegetation and trees. Therefore, both visual- and LiDAR-based SLAM are expected to have difficulty in identifying similarities and correspondences. In addition, IMU position and orientation are expected to drift with time.

Figure 3 and 4 shows the BLK2GO scans following a loop pattern and returning to the same point. Two loops were obtained to get a complete point cloud of the levees (Figure 2a), but the mismatches of one loop are shown in Figures 3 and 4. Large mismatches are found at the starting / ending location both horizontally and vertically. We attribute this to the outdoor environment and the long length (hundreds of meters) of the surveyed levee segment. Identifying and removing such distortions can be challenging, as there are no time tags associated to the individual points of the point cloud.

4. DISTORTION REMOVAL

To remove the geometric distortions identified in the SLAM LiDAR data, an empirical approach was utilized that relies on reference TLS point cloud data and requires manually identified common points found in both datasets. The TLS data are used as reference, as it a trusted surveying technique with high accuracy. Note that in future data acquisitions only SLAM-LiDAR need to be collected, and distortion correction of the SLAM data will be based on the reference TLS dataset showed here; thus increasing monitoring efficiency. The manual identification of common points has the potential to be automated in the future, enhancing the algorithm’s efficiency and applicability for levee monitoring. The flowchart in Figure 5 summarizes the main algorithm steps for removing point cloud distortions due to drift.

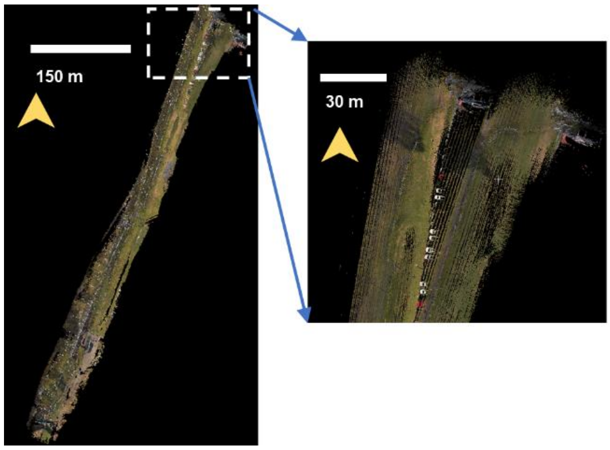

Figure 3. Horizontal mismatch in the SLAM data for loop 1.

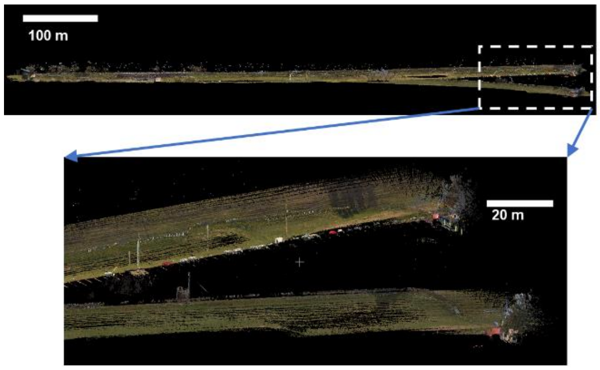

Figure 4. Vertical mismatch in the SLAM data for loop 1.

The initial step is to approximately register the SLAM LiDAR point cloud to the TLS reference. To facilitate efficient algorithm processing, a segment of around 10-20 m in length is selected from one of the two ends of the SLAM point cloud and identified as the “start” of the SLAM data. Based on visual inspection of the data, we assume that distortions present in the initial 10-20 m segment is minor. An iterative closest point (ICP) (Besl and McKay 1992) fit is conducted as implemented in Cloud Compare (Cloud Compare 2015). Figure 6 shows an example of this initial alignment between the TLS data and the SLAM LiDAR data of the first scan line shown in Figure 2b. Figure 6d shows the segment that was used for the initial alignment, while Figures 6a, 6b, and 6c highlight the mismatches between the TLS and the SLAM data at the other end of the dataset.

Next, manual identification of points takes place, and the coordinates of the TLS and SLAM point cloud are recorded. Because the approach was developed for outdoor environments, where there is an absence of easily identifiable objects, identification of corresponding points is expected to be challenging. Our experience so far indicates that approximate identification at the one-meter level is sufficient; although, more accurate identification of corresponding points should be sought, if possible. Figure 6a shows 17 points that were identified in the TLS and SLAM datasets for the first scan line of Figure 2b.

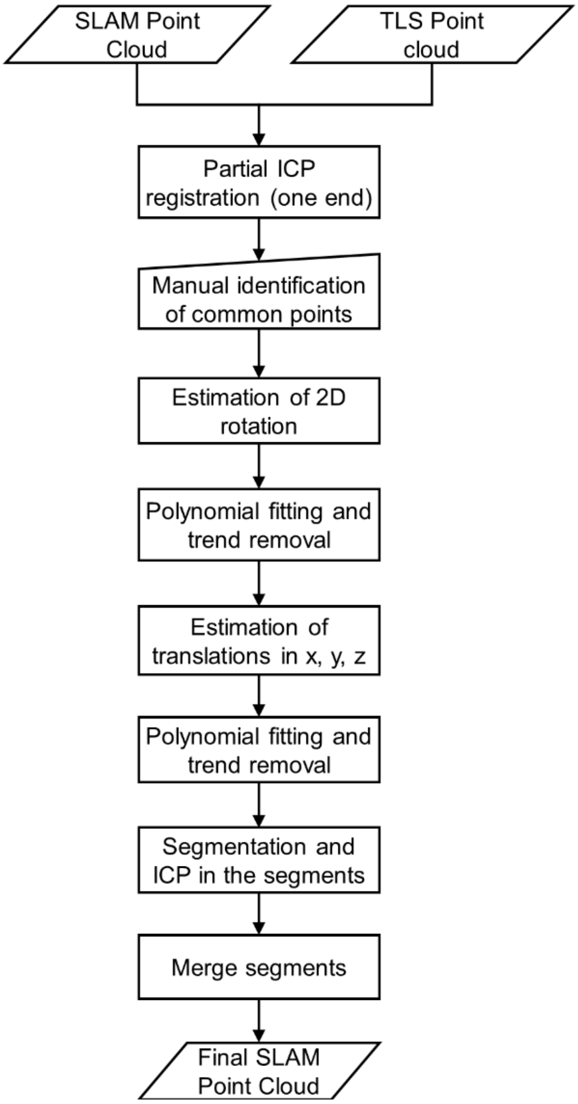

Figure 5. Algorithm flowchart for registering the SLAM point cloud onto the TLS point cloud.

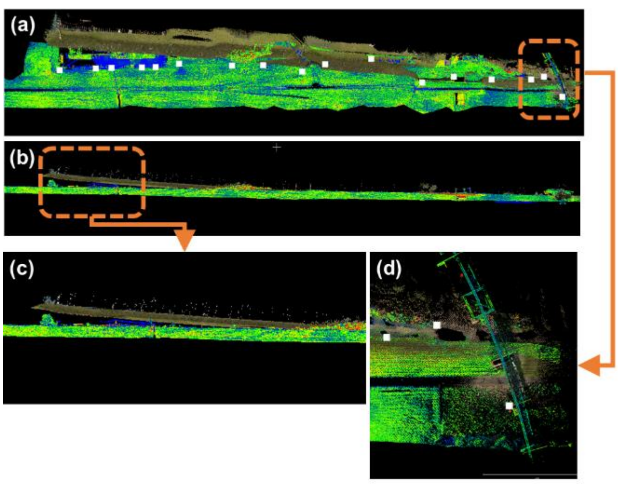

Figure 6. Initial ICP registration between the TLS and SLAM LiDAR data using the ending segment of the first scan line. (a) top view showing the manually identified common points (white squares) in the TLS and SLAM datasets; (b) profile view; (c) cropped view of (b) highlighting the vertical mismatch after initial registration in the one side of the scan line; (d) segment used for initial ICP registration.

In the next step, using the first identified point as reference (e.g., we use the rightmost point in Figure 6a as reference), we compute the azimuth of each point with respect to that reference point. This is done for both the TLS and SLAM points. The difference between the two azimuths corresponds to a 2D angle of rotation for each line. The rotations values for each line are plotted against their distance from the starting point, and a polynomial model is fitted to de-trend the point cloud (Figure 7a).

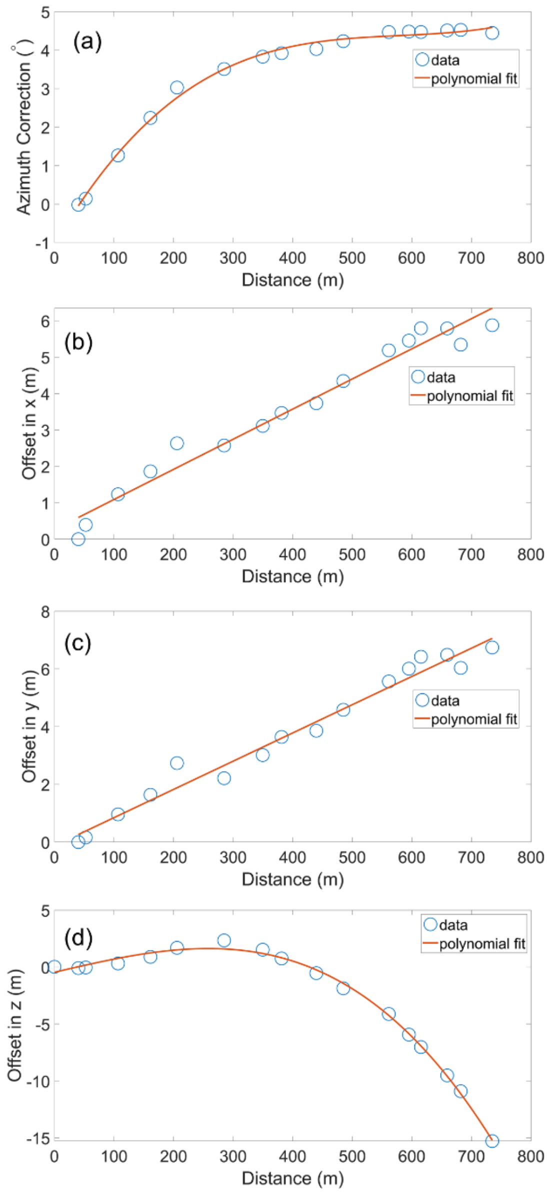

Figure 7. Polynomial fit for drift correction (a) azimuth correction; (b) offset in x-axis; (c) offset in y-axis; (d) offset in z-axis.

In addition, we compute the translations in each direction i.e., x- y- and z-axis. The translations are also plotted against their distance from the starting point, and polynomial models are fitted again (Figure 7b,c,d). The polynomial models in our trials have been simple linear models to fourth order polynomials, depending on the drift / distortion in each case. The SLAM point cloud is then de-trended for rotation and translation in the x- y- and z-axis. The following equation shows the four polynomial model corrections that are considered here:

$$Az_{Corr} = \alpha_0 + \alpha_1 D + \alpha_2 D^2 + \cdots + \alpha_n D^n \tag{1a}$$
$$Offset\_x = \alpha_0 + \alpha_1 D + \alpha_2 D^2 + \cdots + \alpha_n D^n \tag{1b}$$
$$Offset\_y = \alpha_0 + \alpha_1 D + \alpha_2 D^2 + \cdots + \alpha_n D^n \tag{1c}$$
$$Offset\_z = \alpha_0 + \alpha_1 D + \alpha_2 D^2 + \cdots + \alpha_n D^n \tag{1d}$$

Where, Az_{Corr} is the correction in the azimuth direction, $Offset\_x$, $Offset\_y$, $Offset\_z$ are offset corrections in the x-, y-, and z-axis. D is the distance of the manually identified points from the reference point, and $\alpha_0, \alpha_1, \dots, \alpha_n$ are polynomial coefficients up to degree n.

At this stage, the SLAM point cloud is well aligned with the TLS point cloud; however, some rotational effects can still be present. Due to the nature of the SLAM-based geometric errors, the resulting distortions are variable along the surveyed alignment, increasing in magnitude with time. Accounting for this behavior and refining the SLAM point cloud registration requires splitting the dataset into 20 m long segments (or longer if the data can support) and performing the ICP analysis and geometric correction for each segment. The individual segments are then merged to form the final registered and corrected SLAM point cloud. The most time consuming part of the algorithm is the manual identification of common points, which takes several minutes (10 to 30 minutes). Future work will include automating the common point identification process.

Our experience with different segmentation sizes, as high as 50 m, has showed little change in the accuracy of the corrected point cloud. This is important to avoid compromising change detection in the presence of considerable levee deformation. In addition, we have tested the algorithm with the initial ICP registration starting at the opposite side, which does not have well defined features (e.g., man-made structures) and the results achieved similar accuracy (within 1-2 cm). Because the algorithm depends on polynomials defined based on point correspondences, the starting side for initial registration has minimal effect. The ICP refinement performed on the individual sub-segments also ensures to reduce any residual rotational issues.

5. TLS AND SLAM COMPARISON

The distortions in the SLAM LiDAR surveys were mitigated using the process described in the previous section. Table 1 shows the root mean square error (RMSE) of the comparison between the TLS dataset and the corrected / de-trended SLAM LiDAR (i.e., the protected side, top side, and river side). The comparison is implemented using the model-to-model cloud comparison (M3C2) algorithm (Lague et al., 2013). The algorithm offers a robust cloud-to-cloud comparison. In all three cases, the developed algorithm successfully removed high magnitude distortions with RMSE values ranging from 13.0 cm to 15.4 cm. We then merged the three SLAM lines to derive a single corrected SLAM point cloud dataset, which has an RMSE value of 13.4 cm. Note that this comparison is performed in a point cloud to point cloud approach. The two datasets are expected to be affected by vegetation in a different way. To account for this, the SLAM and TLS datasets were gridded using a spatial resolution of 30 cm. For each grid cell the minimum point height was selected as the elevation to reduce the effect of vegetation. The TLS and SLAM LiDAR grids were then used to compute revised RMSE values (Table 2). The revised RMSE values dropped by a few centimeters ranging from 10 cm to 11 cm. The merged SLAM point cloud has a revised RMSE of 11.0 cm when compared to the TLS point cloud, which demonstrates a satisfactory agreement between the TLS and SLAM point clouds.

Dataset	RMSE (cm)
Protected side	14.5
Top side	15.4
River side	13.0
Merged	13.4

Table 1. Point cloud comparisons between the de-trended SLAM lines and TLS. Comparisons are point cloud to point cloud.

Dataset	RMSE (cm)
Protected side	11.1
Top side	11.2
River side	10.5
Merged	11.0

Table 2. Point cloud comparisons between the de-trended SLAM lines and TLS. Comparisons are based on gridded datasets.

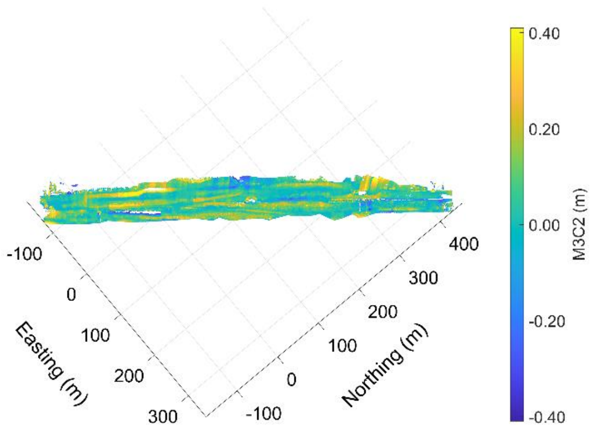

Figure 8. Visualization of the M3C2 distance between the gridded TLS and merged SLAM datasets.

Figure 8 shows a spatial visualization of the M3C2 distances between the TLS and the merged SLAM gridded datasets, while Figure 9 shows the corresponding histogram. Differences between the two datasets are at the 10 cm level with some locations having higher error up to ± 40 cm. Higher differences are mostly noted along the paved trail sections, where there was an absence of TLS data due to data gaps. Figure 10 shows a close-up comparison of the TLS and merged SLAM point clouds in two different locations. Around the building structure we see a good agreement between the two datasets. The power poles show minor alignment issues with differences being up to 0.5 m at the base of the poles. However, of note is that the SLAM point cloud faithfully follows the power lines observed by the TLS point cloud. The figures highlight the successful removal of significant geometric distortions in the SLAM point clouds and the ability to create merged point cloud datasets in outdoor environments with sufficient accuracy for levee inspection and deformation monitoring. Future monitoring will rely on the SLAM-based point clouds using the same TLS point cloud as reference to correct distortions in the successive SLAM datasets.

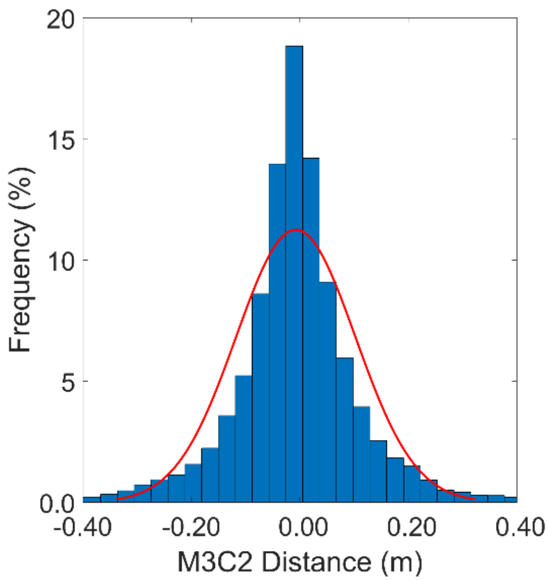

Figure 9. Histogram of the comparison between the gridded TLS and merged SLAM datasets.

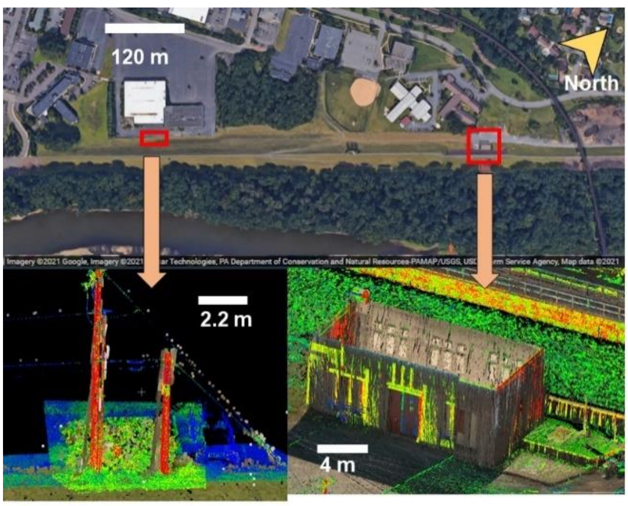

Figure 10. Close up snapshots of the TLS point cloud overlayed on the merged SLAM point cloud. The TLS point cloud is represented as ‘False’ colors based on intensity, and the merged SLAM point cloud as RGB colors.

6. CONCLUSIONS

Advancements in point cloud technologies provide datasets with unprecedented quality and resolution, which are critical for multi-epoch monitoring of engineering structures. In recent years, SLAM technology has seen significant improvement, now able to provide point clouds with cm-level accuracy in indoor environments. However, in outdoor environments successful operation of SLAM LiDAR is challenging due to the absence of well-defined objects (e.g., walls forming planes, and intersection of planes) that can be used by the SLAM algorithm to identify mismatches and correct distortions. TLS and sUAS photogrammetry can provide more accurate and consistent point clouds in outdoor environments than SLAM solutions; however, they present some significant shortcoming in terms of data acquisition. For instance, TLS requires more time spent in the field (e.g., days), and flying a sUAS over levee alignments can create unnecessary risk for the public and can sometimes require time-consuming flight approvals.

This paper combined SLAM and TLS technologies for multi-epoch monitoring of levees. A custom algorithm was developed that is based on an existing TLS point cloud that is used as reference. The SLAM LiDAR must be collected in individual, one-way lines, as opposed to closing the loop to allow correction of distortions as a function of the distance from the starting point. Point correspondences between the TLS and SLAM point clouds are then identified and used to remove distortions using polynomial models in the azimuth direction, and the x-, y-, and z-axis. Results indicate that the initial misalignment of several meters was successfully reduced to a level of ±10 cm, and a merged SLAM point cloud was created to model the levees. Future monitoring of this levee site will rely on SLAM LiDAR point clouds that are corrected using the same TLS dataset (i.e., additional TLS surveys are not necessary for the study site). This can considerably reduce time spent in the field and increase efficiency of monitoring, making SLAM scanning more attractive for long term monitoring.

The algorithm developed in this paper was based on manual identification of point correspondences. In the future the authors will attempt to automate this step of the algorithm to automatically derive point correspondences and incorporate other features such as planes. In addition, more datasets will be collected to expand the evaluation and assessment of the developed algorithm.

ACKNOWLEDGEMENTS

The following undergraduate students are thanked for their assistance in the TLS and SLAM data collection: Gregory Ellsworth, Gerald Rusek, Hannah Corson, Nicholas Lawler, Tyler Pokrinchak, and Tanner Smith.

This project was co-funded by the Luzerne County Flood Protection Authority, and University Name Hidden through Chancellor Endowment Funds.

REFERENCES

Akiyama, N., Nishiyama, S., Sakita, K., Song, J., Yamazaki, F. 2021. River Levees Monitoring Using Three Dimensional Laser Point Clouds with SLAM Technology. In *Civil Infrastructures Confronting Severe Weathers and Climate Changes Conference*, 14-22.

Bakuła, K., Ostrowski, W., Szender, M., Plutecki, W., Salach, A., Górski, K. 2016. Possibilities for using LiDAR and photogrammetric data obtained with an unmanned aerial vehicle for levee monitoring. *Int. Arch. Photogramm. Remote Sens. Spatial Inf. Sci.*, 41.

Bakuła, K., Pilarska, M., Salach, A., Kurczyński, Z. 2020. Detection of Levee Damage Based on UAS Data—Optical Imagery and LiDAR Point Clouds. *ISPRS International Journal of Geo-Information* 9(4), 248.

Besl, P. J., McKay, N. D. 1992. Method for registration of 3-D shapes. In *Sensor fusion IV: control paradigms and data structures, International Society for Optics and Photonics*, 1611, 586-606

Bolkas, D., Naberezny, B., Jacobson, M. G. 2021. Comparison of sUAS Photogrammetry and TLS for Detecting Changes in Soil Surface Elevations Following Deep Tillage. *Journal of Surveying Engineering*, 147(2), 04021001.

CloudCompare 2015. CloudCompare Version 2.6.1 User manual. http://www.cloudcompare.org/doc/qCC/CloudCompare%20v2.6.1%20-%20User%20manual.pdf (10 December 2021)

Lague, D., Brodu, N., Leroux, J. 2013. Accurate 3D comparison of complex topography with terrestrial laser scanner: Application to the Rangitikei canyon (NZ). *ISPRS Journal of Photogrammetry and Remote Sensing* 82, 10-26.

Leica Geosystems, A. G. BLK2GO for DTM generation in highly vegetated area for detecting and documenting archaeological earthwork anomalies. In *IMEKO TC-4 International Conference on Metrology for Archaeology and Cultural Heritage*

Leica Geosystems 2021a. BLK2GO. https://shop.leica-geosystems.com/learn/blk2go/blk2go-technology (10 December 2021)

Leica Geosystems 2021b. Leica ScanStation P50 – Long Range 3D Terrestrial Laser Scanner https://leica-geosystems.com/en-us/products/laser-scanners/scanners/leica-scanstation-p50 (10 December 2021)

Lenac, K., Kitanov, A., Cupec, R., Petrović, I. 2017. Fast planar surface 3D SLAM using LIDAR. *Robotics and Autonomous Systems* 92, 197-220.

Zou, Q., Sun, Q., Chen, L., Nie, B., Li, Q. 2021. A Comparative Analysis of LiDAR SLAM-Based Indoor Navigation for Autonomous Vehicles. *IEEE Transactions on Intelligent Transportation Systems*.